TOWARDS PREPARATION CONDITIONS FOR THE SYNTHESIS OF ALKALI-ACTIVATED BINDERS USING TUNGSTEN MINING WASTE

Gediminas Kastiukas[1], Xiangming Zhou[2,*], and João Castro-Gomes[3]

[1]Department of Mechanical, Aerospace and Civil Engineering, Brunel University London, Uxbridge, Middlesex UB8 3PH, United Kingdom

[2]Department of Mechanical, Aerospace and Civil Engineering, Brunel University London, Uxbridge, Middlesex UB8 3PH, United Kingdom

[3]Centre of Materials and Building Technologies, University of Beira Interior, 6200 Covilhã, Portugal

*(Corresponding author) e-mail: Xiangming.Zhou@brunel.ac.uk

ABSTRACT

This study evaluated the results of preparation conditions for the production of an alkali-activated binder (AAB) based on a binary mixture of tailings from tungsten mine waste (TMW), and waste glass (WG) activated with a mixture of sodium silicate (SS) and sodium hydroxide (SH). 40 wt.% WG increased the amorphous nature of the binary blend by 21% without initiating the alkali-silica reaction. SS/SH activator solution was subjected to a variation of mixing times, and its sensitivity was measured using temperature monitoring, and Fourier Transforms Infrared Spectroscopy (FTIR). After 20 minutes of mixing, the SS/SH activator solution showed a 3.13°C reduction in temperature, a 21.4% increase in unbound water content and as a result imparted a 26% drop in the mechanical resistance of TMW-WG AAB at 28-days. The TMW-WG AAB was also determined to develop the highest compressive strength when cured at 80°C for 24h in sealed conditions. The following conditions, supported by X-ray diffraction (XRD) and Fourier transforms infrared analysis (FTIR), are responsible for the most significant dissolution of the alumino-silicate oxides.

Author keywords: alkali-activated binder; binary blend; curing temperature; geopolymer; material preparation; mixing time; precursor reactivity; synthesis conditions; tungsten mining waste; waste glass

INTRODUCTION

Although the development of Portland cement (PC) research and its application has considerably matured in last few decades, it is still facing challenges due to its impact on the environment. The production of cement is one of the industry's most energy intensive processes next only to steel and aluminium (Napp et al. 2014). In 2011, the European states accounted for 7.6% of total global cement production (European Cement Association 2014). The manufacture of PC can consume approximately 3.2-6.3 GJ of energy (thermal and electrical) per tonne of clinker product (Rahman et al. 2016) with almost half of this being used for the fine grinding of clinker to make the cement. The main raw material used in cement production has traditionally been the abundantly available limestone which, by its inevitable transformation into lime, is responsible for over 60% of the cement industry's CO_2 emissions (Mikulčić et al. 2012). For every kg of PC clinker produced, about 0.87 kg of CO_2 is released (Telesca et al. 2017). Therefore, the main challenge of the cement industry is focused on the CO_2 emission reduction to 1.55 Gt per year (about 45% of the current value) by 2050 (Telesca et al. 2017).

To reduce the carbon footprint and conveniently dispose of the variety of waste material available from multiple industries, alkali-activated binders (AABs for short hereafter) have attracted increasingly more attention from the scientific community as environmentally favourable alternatives to PC (Barbosa et al. 2000; Bădănoiu et al. 2015). Aluminosilicate rich materials can be chemically activated to produce a three-dimensional polymer like network containing both crystalline and amorphous phases (Davidovits 1981). These

particular binders yield high strength with rapid setting, good durability and high resistance to chemical attack (Hardjito et al. 2009; Ariffin et al. 2013; Thomas and Peethamparan 2015). Despite the existence of strong economic and environmental drivers, alkali-activated binders are still not widely implemented throughout the world. They represent an attractive alternative for the partial or complete substitution of PC, offering comparable performance (Neupane 2016) and cost (Duxson et al. 2007a) while reducing greenhouse gas emissions (Duxson et al. 2007b).

The raw materials used for synthesising AABs are typically calcined clays or low-calcium fly ashes (Duxson et al. 2007a). However, the supply of fly ash in Europe is in decline due to the industry becoming increasingly less reliant on coal-fired power stations (Carroll 2015) while the disposal of the 85% of host rock generated from kaolin clay mining is an increasingly critical issue (Murray 2002). On the other hand, mining and quarrying waste still represent 15% of the total waste in Western Europe and 31% in Eastern Europe (Pacheco-Torgal et al. 2009b), while the USA alone is estimated to produce between 1000-2000 Mt of mining waste annually (Szczepańska and Twardowska 2004). The favourable mineralogical composition of mining waste for alkali activation (Jiao et al. 2013; Ye et al. 2014; Zhang 2014) combined with its continuously large production make it an attractive and environmentally friendly feedstock for AABs.

Some mining and quarrying wastes can be reused in earthworks and construction, in particular, the coarser fractions. Typical applications include use in asphalt pavements (Albuquerque et al. 2006; Akbulut and Gürer 2007) and concrete (Yellishetty et al. 2008; Hebhoub et al. 2011). However, recent studies on the reuse of fine tailings as raw material for AABs are considered to be most promising; from an environmental, technical and economic point of views. For this study, the wastes of particular interest are fine tailings derived from tungsten mining. Preliminary research has been conducted on the transformation of this type

of waste into AABs and has shown promising results. Pacheco-Torgal et al. (2007) first highlighted the potential of using calcined tungsten mining waste mud blended with calcium hydroxide for the development of a high early strength geopolymeric binder. Tungsten mining waste also identified to be very effective for stabilizing/solidifying heavy metals particularly when used in conjunction with blast-furnace slag (Choi et al. 2009) and overall, suggested that mortar with acceptable properties can be developed using up to 10% by mass tungsten mining waste. Later, alkali-activated artificial aggregates were produced from such mining waste mud, and their properties were studied as a potential substrate for fixed-film wastewater treatment processes (biofilm reactors). The results showed that the aggregates obtained have suitable resistance to acid attack and may be used as a substrate for fixed-film biological reactors for the treatment of acid wastewaters (Silva et al. 2012a). Also, mine tailings blended with other industrial by-products such as fly ash have resulted in the production of an AAB with high compressive strength, mainly due to the Si/Al ratio of the raw material blend falling within the optimum Si/Al ratio for alkali-activation (Zhang et al. 2011; Ahmari and Zhang 2012).

Despite the research conducted so far, it remains that tungsten mining waste possesses a low degree of reactivity due to it crystalline phases. Thermal treatments have previously been studied to improve the amorphicity of tungsten mining waste, and satisfactory strengths have been achieved (Pacheco-Torgal et al. 2009b), nonetheless at the expense of the high amount of energy. A more sustainable method would be to blend the tungsten mining waste with a material that would increase not only its level of amorphicity but also maintain its environmental appeal. In this case, waste glass would be the ideal candidate since it is a very common construction and household waste material with a highly amorphous structure. It is estimated that out of 18 million tonnes of glass wastes accumulated in 2012 in the EU, only 35% of this was recycled (Glass for Europe 2013). The feasibility of using ground waste

glass to improve mechanical performance has already been achieved with PC concrete (Shao et al. 2000a) and initiated with metakaolin based AABs (Christiansen and Sutter 2013).

Also when assessing novel binder materials, it is of as much importance to study the preparation/manufacturing techniques as it is the final material properties. This is a domain which currently remains understudied for AABs in general, let alone those based on tungsten mining waste.

Thus, the primary objective of this study is to determine the fundamental aspects of AAB synthesis using tungsten mining waste as the principle raw material with the added feasibility of its partial replacement by waste glass. Particular focus will be on (1) the influence of waste glass on tungsten mining waste reactivity; (2) alkali activator solution preparation and kinetics; (3) AAB curing temperature and curing duration.

MATERIALS AND METHODS

Materials

The raw materials used in this investigation consisted of tungsten mining waste (TMW), waste glass (WG), sodium hydroxide (NaOH) (SH), and sodium silicate (Na_2SiO_3) (SS). The TMW was derived in powder form from the Panasqueira mine in Castelo Branco, Portugal, and the WG was received from the local municipality of Covilhã, Portugal. The chemical composition of the TMW and WG as obtained by SEM-EDX (SUPRA 35VP/EDAX). Due to the waste nature and microscopic inhomogeneity of the TMW, chemical analyses were made from different batches collected from the mine. Therefore, the results of TMW reported in Table 1 are the average values accompanied with the standard deviation (S.D). According to Table 1, for TMW, the oxides SiO_2, Al_2O_3, Fe_2O3, and SO_3 are the most abundant, while the oxides SiO_2, MgO, SO_3 and Fe_2O_3 showed the greatest variability. Grain size distribution analysis was performed for the precursor materials after mechanical sieving by laser

diffraction analysis according to BS ISO 13320:2009. The TMW has a mean particle size of 26μm while the waste glass has a mean particle size of 39.6μm. The WG was intentionally used with a slightly larger mean particle size to reduce the energy consumption during the milling process. The bulk powder densities of TMW and WG were determined using a gas displacement pycnometer (AccuPyc II 1340) and were determined as 3.08 and 2.53 g/cm^3, respectively. Sodium hydroxide solution was prepared by dissolving sodium hydroxide pellets (98% purity obtained from Fisher Scientific) in de-ionized water and allowed to cool before use. Sodium silicate (obtained from Solvay SA, Portugal) had a SiO_2/Na_2O = 3.23 (8.60 wt.% Na_2O, 27.79 wt.% SiO_2, 63.19wt.% H_2O, 0.4wt.% Al_2O_3).

Synthesis of samples

All experiments were carried out at 20°C. TMW alkali-activated binders with up to 40 mass-% replacement with WG were blended with an IKA Ultra-Turrax T50 mixer at 360 rpm for 60 s. Based on the research on alkali-activation available in the literature concerning mechanical strength and efflorescence formation potential in AABs combined with the experience gained from previous studies (Pacheco-Torgal et al. 2008; Silva et al. 2012b; Kastiukas et al. 2016), the following ranges were selected for the constituents of the AABs:

- Molarity of SH = 10M
- Weight ratio of SS/SH = 4
- Weight ratio of precursor/activator = 3.6

The following ratios produced an AAB with a flowability of 130 ± 5mm determined using the method proposed by EN 1015-3:1999 (2006) and initial and final setting times of 90 and 110 minutes determined EN 196-3 (European Committee for Standardization 2005). In the precursor/activator ratio, the precursor is the TMW and WG, and the activator is the solution containing the alkali, the silicate and the water.

To produce the TMW-WG AAB, the TMW, and WG were mixed in the dry state for five minutes, forming the precursor materials. The sodium hydroxide and sodium silicate solutions were mixed for a period ranging from 2.5 to 60 mins at 700 rpm, depending on the type of condition being tested, forming the alkali activator. The alkali-activator solution was slowly added to the precursor materials, and the resulting paste was stirred for 2.5 minutes at 200 rpm, followed by 2.5 minutes at 400 rpm. The resulting AAB was then placed in 40x40x160 mm^3 prismatic Styrofoam moulds. The mould was filled with the AAB in three stages and manually vibrated after each successive filling stage to release trapped air bubbles, and sealed with a film to avoid the loss of water and ingress of CO_2. Samples which were made to test curing exposed to the atmosphere were cured unsealed. The specimens were placed in a temperature and humidity controlled environmental chamber at 50% RH for curing between 20 and 80°C for 4-36h, depending on the type of condition being tested. After curing, prisms were de-moulded and left in a laboratory condition of 20°C for curing until the test age. The specimens cured at 20°C were de-moulded after 48 h due to a slow setting. Table 2 summarises synthesis conditions tested in this study i.e. activator solution mixing time, curing temperature and curing time.

To observe for chemical changes in the activator solution during mixing, the first it was decided to isolate the activating solution and monitor its temperature during the mixing process. The temperature evolution of the activator solution was measured using the setup shown in Fig. 1. The activator solution was prepared at the same SS/SH solution ratio as that used to make the TMW-WG ABB i.e. 4.0. A polystyrene enclosure was used to contain the activator solution and provided a thermodynamically stable environment. Two K-type thermocouples with the tips wrapped in temperature sensitive copper tape were connected to a multi-channel data logger and used to measure the temperature of the activator solution and

enclosure's interior, respectively. Once the activator temperature was deemed constant, mixing was started and continued for 20 minutes at 700 rpm.

Compressive Strength

The demoulded samples were left to rest at 20°C and a relative humidity of 75 % until the specific age of testing. The compressive strength of the prismatic sample fractured counterparts was tested after 1, 3, 7, 28 days in accordance with EN 196-1 using a universal testing machine (Instron 5960) at a constant loading rate of 144 kN/min. The compressive strength value was the average of values obtained from three specimens.

X-ray Diffraction (XRD) Analyses

The mineralogical compositions of the TMW and WG were obtained by powder X-ray diffraction (BRUKER D8 Advance) with an automatic slit, monochromated CuKα radiation (λ=1.5405 Å), 5-80° 2θ range, 0.600 s count time, Cu radiation, 40kV and 40mA. Peak shapes were studied using the program DIFFRACT.SUITE.

Fourier Transform Infra-Red (FTIR) Analyses

FTIR spectra were recorded from 400 to 4000 cm^{-1} with a $2cm^{-1}$ resolution, 5 kHz scanning speed and 25 scan count using a Shimadzu IRAffinity-1 fitted with a Specac Quest attenuated total reflectance (ATR) accessory.

Scanning Electron Microscopy (SEM)

Microstructural studies utilised SEM (Zeiss Supra 35VP) equipped with EDS analyser (EDAX). Backscattered and Secondary electron images were collected from polished specimens to overcome the main limitation of fracture surfaces. To prepare the polished specimens, 5-mm-thick slices were cut using a low-speed saw. The samples were first impregnated with ultra-low viscosity resin and then polished.

Stopping the activation process

Both the XRD and FTIR samples were tested in a state where the alkali activation process was stopped using the combined water and solvent extraction protocol developed by Chen et al. (2014). In summary, it involved stirring the AAB specimen in deionized water and then removing the liquid by centrifuging. Upon addition of methanol, soluble silicate species could be observed in the liquid layer. Thus water extraction by centrifuging was used to remove the precipitates. Specimens were then ground to micron-sized particles using a mortar and pestle, and a solvent of methanol/acetone mixture was added, followed by further grinding. The solvent was removed using vacuum filtration; this latter procedure was repeated for five times.

RESULTS AND DISCUSSION

Influence of Waste Glass on Tungsten Mining Waste Reactivity

The recorded FTIR spectra of raw TMW and WG and blended as TMW/WG are shown in Fig.2. For the spectra of WG, the highest absorption coefficient is associated with the Si-O bending vibration near 453 cm^{-1}. A weaker band due to the bending mode near 1000 cm^{-1} is accompanied by the still weaker feature near 775 cm^{-1}. For the TMW, the highest absorption coefficient is associated with the bending vibration of the Si-O between 465 and 424 cm^{-1}. Weaker features are associated with the bending vibration of Si-O at 984 cm^{-1} and its symmetric stretching vibration between 797 and 694 cm^{-1}. The weakest bands at 827cm^{-1} and 1163 cm^{-1} can be associated with the bending of the Si-O bond of the original TMW. The absorbance spectrum of the TMW/WG blend displays the same spectral bands as the raw TMW, only at lower intensities, obviously due to the combination of different intensities.

Results of the XRD analyses shown in Fig.3 reveal that the TMW precursor material predominantly consists of muscovite and silica with traces of sodium aluminosilicate,

rudashevskyite and pyrite and is similar to the TMW chemical composition identified by Pacheco-Torgal et al. (2009). The WG is revealed to consist of silica, lime and sodium oxide with traces of potassium and iron oxide. Using a general non-linear least squares system software (TOPAS V5), the TMW and WG were determined to be 97% and 15% crystalline, respectively. Compared to other materials commonly used as AAB precursors such as fly ash (Van Jaarsveld and Van Deventer 1999) and metakaolin (Provis et al. 2005), the TMW is of a far less amorphous nature. In this study, a sustainable approach was chosen to increase the amorphicity of the TMW through the addition of WG. The addition of 40 wt.% WG led to an increase in the amorphicity, qualitatively indicated by the more intense amorphous background from 15° to 45° in the TMW/WG blend XRD spectrum and also by a 21% calculated reduction in crystallinity. The compressive strength of TMW-WG AAB was used to evaluate the strength contribution potential as a function of the degree of amorphicity. Thus Fig.4 shows the evolution of compressive strength in TMW-WG AAB with 20, 30 and 40 wt.% WG replacement over 28 days. The results obtained for pure TMW AAB are also included. Each reported result corresponds to the average measurement in three specimens per each WG replacement value and age; the deviation of results fluctuated between 0.22 and 1.4%. In Fig.4 it can be observed the compressive strength increased with an increase in the WG content at all ages. The highest 28-day strength was obtained by the 60TMW40WG sample at 41MPa, which is 127% higher than the control sample 100TMW. The compressive strength would be influenced primarily by the additional release of reactive silica. However, it also expected that the CaO content in the WG would contribute to the strengthening of the reaction products, most likely in the form of a (C, N)-A-S-H gel.

The compressive strength results with the highest replacement level of WG i.e. 40wt.% is consistent with the compressive strength results previously obtained by Pacheco-Torgal et al. (2009b), specifically 39.6 MPa at 28 days, for mortar prepared with TMW. However, this

was achieved only after an energy intensive calcination treatment of the TMW at 950°C for 2 hours.

Finally, the reactive silica-containing WG combined with the highly alkaline activator solution may create the potential for the deleterious process of alkali-silica reaction (ASR) and required validation. TMW-WG AAB with the highest replacement of WG i.e. 40 wt.% was stored at a RH of 80% at 38°C to accelerate the ASR reaction; a thin-section of this sample shown in Fig.5. Observation of the section, which is representative of the WG as a whole, revealed that there were no signs of ASR gel formation around the WG particles or in the open voids. Data reported in the literature established that if the waste glass is ground under 75 μm, the ASR effect does not occur, and binder durability is guaranteed (Shao et al. 2000b). Water is also a necessary condition for ASR; considering the TMW-WG AAB only required a water/precursor demand of 0.179, this may also be the reason for the absence of ASR.

Alkali Activator Preparation Conditions

To prepare the TMW-WG AAB, it is necessary that the alkali activator is in a homogeneous state upon mixing with the powder precursors. Fig.6 shows the effect of activator mixing time on the 80TMW20WG AAB compressive strength. It can be seen that the 28-day strength increases when using the activator which has been mixed between 2 and 5 minutes only (i.e. M2.5 and M5), reaching the maximum 28-day strength of 17 MPa at an activator mixing time of 5 minutes (i.e. M5). As the activator mixing time is extended, an immediate drop in compressive strength is observed. The activator solution mixing time has a strong impact on the 28-day strength, as a 26% drop in compressive strength is recorded for the TMW-WG AAB when prepared using an activator solution stirred for 20 minutes i.e. M20. Fig.7 presents the results of the activator solution temperature during mixing. The black and red curves represent the activator and enclosure air temperature, respectively. Over the course of

20 minutes of mixing, an average reduction of 3.13°C in activator temperature was recorded from three identical tests, while the enclosure temperature was recorded to remain stable at 23°C±0.1°C. This drop activator solution temperature is an endothermic process resulting from the reorientation of the water molecules, leading to a disruption of the hydration shells surrounding the ions. The positive metal ions, in this case, Na^{+}, are particularly at risk since they inherently possess weaker attractions to the negative oxygen end of the water molecule. The prolonged mixing can be thought to cause a net stripping effect of the water molecules from the ions. The latter would impact the dissolution and subsequent mobility of the siliceous material present in TMW and WG, leading to a less intense attack on the silicon-oxygen bonds and thus a reduction in mechanical performance, as verified by the results in Fig.6.

Further interpretation of this is shown by the ATR-FTIR spectra of the activator mixed for 5 and 20 minutes in Fig.8. The 3270cm^{-1} band (which is a sensitive and well-defined band corresponding to the O-H vibrations in water) is revealed to increase in intensity by 21.4%, which based on literature concerning FTIR spectra of water at different temperature (Praprotnik et al. 2004), may be considered as a significant amount. It is an indication that the activator solution mixed for 20 minutes possesses a higher unbound water content with fewer solvated ions and more available as free molecules. Also, visually observed after 20 minutes of mixing was the partial gelation of the soluble silicate anions detected by the loss of uniform fluid flow and the adherence of solid gel to the glass wall. Polymerization of silicates commonly occurs at pH close to neutral, but can also be triggered by an increased water content (Hu et al. 1993). Gelation would also contribute to reducing the effectiveness of the activator to balance the charge of the aluminate groups in the phyllosilicate, resulting in a negative effect on the kinetics of the reaction and therefore the development of mechanical strength. From a practical outlook, it must be emphasised that the preparation of the alkali

300 activator is independent of the mixing of the final binder. Therefore, the alkali-activators
301 dependence on mixing time should not be considered to interfere with the upscaling potential
302 of AABs.

303 **TMW-WG AAB Curing Temperature and Curing Time**

304 Samples T20 through to T80 in Table 2 were made so that the effect of different curing
305 temperatures on compressive strength of TMW-WG AAB could be studied. The prisms cast
306 were cured under sealed conditions at 20, 40, 60 and 80°C for 24h, then tested for
307 compressive strength after 1, 3, 7 and 28 days. The compression strength results in Fig.9
308 present details on the role of temperature on the properties of TMW-WG AAB. The
309 compressive strength of all the samples at all ages increased with increasing curing
310 temperature. Samples cured at 20°C (i.e. T20) did not develop appreciable compressive
311 strength for the first 7 days of curing and were only able to attain 2.6 MPa after 28 days. The
312 highest compressive strengths were obtained by curing at 80°C (i.e. T80), allowing the
313 TMW-WG ABB to attain 22MPa at 28 days. From this, it can be concluded that the reaction
314 that took place was a temperature-driven process. Van Jaarsveld et al. (2002) and Bakharev
315 (2005) reported comparable compressive strength results for fly ash based AABs. Curing the
316 samples above 80°C was not attempted due to the sufficient strength gained from curing at
317 80°C. Higher temperatures would also require a greater energy input; a factor this study
318 wanted to avoid by keeping the production of the binder as less energy intensive as
319 practically possible.

320 Fig.10 shows the FTIR spectra of the TMW/WG blend of raw materials and the TMW-WG
321 AAB cured at different temperatures (i.e. T20-T80). The TMW-WG AAB cured at 20°C (i.e.
322 T20), as expected, displays the highest absorbance, which can be inferred as reduced
323 hardening activity and thus slow strength development. The spectra of samples cured at 40

and 60°C (i.e. T40 and T60) match each other closely indicating similar molecular structures are present in both samples when curing at the respective temperatures. However, the change in absorbance for the sample cured at 80°C (i.e. T80) is more evident. The latter spectrum shows a great reduction in absorbance and broadening between 850 and 1100 cm^{-1} associated with the Si–O-Si symmetric stretching vibrations for the gel product and is an indication of increased activation. A similar feature can be observed at 775 and 694 cm^{-1}, the region of the spectrum also representing symmetric stretching vibration of the raw material Si-O bonds. The development of a more amorphous gel phase with the increase in curing temperature can be inferred from the spectrum of the TMW-WG AAB sample at 80°C matching that of the raw WG, which is confirmed to be inherently amorphous from the XRD results (refer to Fig.3). Nonetheless, the presence of asymmetric stretching vibration (Si–O–Si) related to non-solubilised particles at ~1000 cm^{-1} and ~450 cm^{-1} in the TMW-WG AAB indicates that unreacted precursor materials are still present, supporting the same result found in the XRD analysis. Milling the precursor materials to a fine particle size has been shown to improve reactivity and dissolution in an alkali activator solution. In the case of fly ash, Temuujin et al. (2009) showed that vibration milling could reduce the median particle size by more than 50% and improve the compressive strength by 80%. This method of mechanical activation could potentially be used to improve the dissolution properties of TMW further, as long as the additional energy input did not compromise the low energy potential of the TMW-WG AAB.

Just as important as curing temperature is the AAB heat curing duration. Samples D4 through to D36 in Table 2 were prepared to study the effect of curing time on the compressive strength of TMW-WG AAB. Samples were cured in sealed conditions for 4, 12, 24 and 36h at 80°C and tested for compressive strength after 1, 1.5 (36h), 3, 7 and 28 days. Fig.11 shows that the compressive strength improves with an increase in curing time from 4 to 24h. The improvement in compressive strength continues at an even higher rate when the curing time

increases from 12 to 24h. However, after 36h of curing a depreciation of the compressive strength at 36h (identified by the yellow marker in Fig.11), 3 days and 7 days is observed, leaving the 28-day strength unchanged. Thus, it can be concluded that the activation reaction that took place was time-dependent. Fig.12 shows the SEM images of TMW-WG AAB samples cured at 80°C for 24 and 36h. The microstructure of the sample cured for 24h consists of close-packed quasi-unreacted WG particles embedded in a continuous matrix of gel products while the sample cured for 36h exhibits visible contraction, particularly around the WG particles. Although samples were kept in sealed conditions during curing, it was observed during de-moulding that some water was still able to evaporate into the surrounding air within the curing bag. Previous work by Mo et al. (2014) suggested that the contraction of AAB samples cured under sealed conditions at 80°C occurs after 7days. However, the results of this study suggest that contraction can initiate as early as 36h. It is possible that prolonged exposure to the elevated temperature may have led to the water evaporation rate being greater than that of re-saturation, thus triggering the accumulation of internal stresses and subsequent contraction of the AAB matrix.

The absorbance spectra for the raw TMW/WG blend and TMW-WG AAB, cured for varying periods of time (i.e. D4-D36) are shown in Fig.13. A reduction in the absorption intensity of the main bands at ~1000, ~775 and ~446 cm^{-1} indicates that longer curing times led to the further dissolution of Si-O from the raw materials. Also, the position of Si-O bending vibration peaks shifted from 999 and 463 cm^{-1} in the raw TMW/WG to 989 and 446 cm^{-1} respectively for the TMW-WG AAB specimen cured for 24h, a type of shift associated with a greater extent of polymerization in aluminosilicates (Sarkar et al. 2015). Also, it is important to observe that the absorbance spectrum for the TMW-WG AAB sample cured for 24h (i.e. D24) displays lower absorbance intensities than the TMW-WG AAB sample cured for 36h. It can be inferred from this latter result that curing times above 24h can lead a reduction in Si-O

374 dissolution and complements the mechanical strength results in Fig.11 which clearly show
375 reductions in compressive strength for samples cured for 36h. Previous research regarding the
376 curing time of AAB's made from fly ash (Li et al. 2013) and metakaolin (Heah et al. 2011)
377 have uncovered similar results. Also, the broadening of the characteristic bands between
378 1100-850 cm^{-1} and 800-750 cm^{-1} implies the overlap of more bands with a higher intensity
379 which in this case is attributed to the asymmetric stretching vibrations of T-O-Si (where T=
380 Si or Al) (Khater 2013).
381
382 **CONCLUSIONS**
383
384 The effect of waste glass addition to tungsten mining waste alkali-activated binders was
385 assessed by strength testing, XRD, SEM and FTIR. Additionally, preparation conditions such
386 as activator mixing time, curing temperature and curing time on hardening kinetics was
387 assessed, leading to the following discoveries:

388 • The addition of WG is a very sustainable and practical method of improving TMW
389 degree of amorphicity, compared to traditional calcination treatments. Up to 40 wt.%
390 of WG with a mean particle size of 39.6μm can be successfully blended with TMW to
391 increase the amorphous nature of the binary blend by 21%, without the initiation of
392 the alkali-silica reaction.
393 • Prolonged activator mixing can reduce the dissolution of the aluminosilicate precursor
394 due to fewer available alkali metal ions in solution. The initiation of silicate gelation
395 due to prolonged stirring would also contribute to reducing the activator effectiveness.
396 The correct preparation of the activator solution is imperative and would be expected
397 to extend to other classes of alkali activated cementitious systems.
398 • The optimum conditions for obtaining the most significant dissolution of the alumino-
399 silicate oxides were curing for 80°C for 24h. When curing time is greater than 24h i.e.

36h as investigated in this study, it can lead to a reduction in compressive strength and contraction of the AAB matrix, even under sealed conditions.

ACKNOWLEDGMENT

Partial financial support from the European Commission Horizon 2020's MARIE Skłodowska-CURIE Research and Innovation Staff Exchange Scheme through the grant 645696 (i.e. REMINE project) is greatly acknowledged. The first author thanks, Thomas Gerald Gray Charitable Trust and Brunel University London for providing fees and a bursary to support his PhD study.

REFERENCES

Ahmari, S., and Zhang, L. (2012). "Production of eco-friendly bricks from copper mine tailings through geopolymerization." *Constr. Build. Mater.*, Elsevier Ltd, 29, 323–331.

Akbulut, H., and Gürer, C. (2007). "Use of aggregates produced from marble quarry waste in asphalt pavements." *Building and Environment*, 42(5), 1921–1930.

Albuquerque, J. C. A., Interior, B., and Silva, A. P. (2006). "Valorização de resíduos de minas em compósitos poliméricos." *CVR*, 45(March 2006), 9–11.

Ariffin, M. A. M., Bhutta, M. A. R., Hussin, M. W., Mohd Tahir, M., and Aziah, N. (2013). "Sulfuric acid resistance of blended ash geopolymer concrete." *Constr. Build. Mater.*, 43, 80–86.

Bădănoiu, A. I., Abood Al-Saadi, T. H., and Voicu, G. (2015). "Synthesis and properties of new materials produced by alkaline activation of glass cullet and red mud." *Int. J. Miner. Process.*, 135, 1–10.

Bakharev, T. (2005). "Geopolymeric materials prepared using Class F fly ash and elevated temperature curing." *Cem. Concr. Res.*, 35(6), 1224–1232.

Barbosa, V. F. F., MacKenzie, K. J. D., and Thaumaturgo, C. (2000). "Synthesis and characterisation of materials based on inorganic polymers of alumina and silica: sodium polysialate polymers." *Int. J. Inorg. Mater.*, 2(4), 309–317.

Carroll, R. A. (2015). "Coal Combustion Products in the United Kingdom and the Potential of Stockpile Ash." *2015 World of Coal Ash (WOCA) Conference*, Nashville, 7.

Chen, X., Meawad, A., and Struble, L. J. (2014). "Method to stop geopolymer reaction." *J. Am. Ceram. Soc.*, 97(10), 3270–3275.

Choi, Y. W., Kim, Y. J., Choi, O., Lee, K. M., and Lachemi, M. (2009). "Utilization of tailings from tungsten mine waste as a substitution material for cement." *Constr. Build. Mater.*, 23(7), 2481–2486.

435 Christiansen, M. U., and Sutter, L. L. (2013). "ACI SP 294 - Advances in green binder
436 systems." *Waste glass for use in geopolymers*, N. Neithalath and J. Hicks, eds., ACI, 31–
437 48.

438 Davidovits, J. (1981). "The need to create a new technical language for the transfer of basic
439 scientific information." *Transfer and Exploitation of Scientific and Technical*
440 *Information*, Luxembourg, 316–320.

441 Duxson, P., Fernández-Jiménez, A., Provis, J. L., Lukey, G. C., Palomo, A., and van
442 Deventer, J. S. J. (2007a). "Geopolymer technology: the current state of the art." *J.*
443 *Materi. Sci.*, 42(9), 2917–2933.

444 Duxson, P., Provis, J. L., Lukey, G. C., and van Deventer, J. S. J. (2007b). "The role of
445 inorganic polymer technology in the development of 'green concrete.'" *Cement and*
446 *Concrete Research*, 37(12), 1590–1597.

447 European Cement Association. (2014). "The role of cement in the 2050 low carbon
448 economy." <http://www.cembureau.be/role-cement-2050-low-carbon-economy> (Jul. 5,
449 2016).

450 European Committee for Standardization. (2005). *Methods of testing cement - Part 3:*
451 *Determination of setting times and soundness*.

452 European Standard. (2006). *Methods of test for mortar for masonry — Part 3: Determination*
453 *of consistence of fresh mortar (by flow table). EN 1015-3:1999. BS EN 1015-3:1999*
454 *+A2*.

455 Glass for Europe. (2013). "Recycling of end-of-life building glass." <goo.gl/CzmEvs> (Jan.
456 8, 2017).

457 Hardjito, D., Cheak, C. C., Ho, C., Ing, L., and Ing, C. H. L. (2009). "Strength and Setting
458 Times of Low Calcium Fly Ash-based Geopolymer Mortar." *Mod. Appl. Sci.*, 2(4), 3–
459 11.

460 Heah, C. Y., Kamarudin, H., Bakri, A. M. M. Al, Binhussain, M., Luqman, M., Nizar, I. K.,
461 Ruzaidi, C. M., and Liew, Y. M. (2011). "Effect of Curing Profile on Kaolin-based
462 Geopolymers." *Physics Procedia*, 22, 305–311.

463 Hebhoub, H., Aoun, H., Belachia, M., Houari, H., and Ghorbel, E. (2011). "Use of waste
464 marble aggregates in concrete." *Construction and Building Materials*, Elsevier Ltd,
465 25(3), 1167–1171.

466 Hu, Y., Chung, Y. J., and Mackenzie, J. D. (1993). "Gelation kinetics of an organically
467 modified silicate." *Journal of Materials Science*, 28(24), 6549–6554.

468 Van Jaarsveld, J. G. ., Van Deventer, J. S. ., and Lukey, G. C. (2002). "The effect of
469 composition and temperature on the properties of fly ash- and kaolinite-based
470 geopolymers." *Chem. Eng. J.*, 89(1–3), 63–73.

471 Van Jaarsveld, J. G. S., and Van Deventer, J. S. J. (1999). "Effect of metal contaminants on
472 the formation and properties of waste-based geopolymers." *Cem. Concr. Res.*, 29(8),
473 1189–1200.

474 Jiao, X., Zhang, Y., and Chen, T. (2013). "Thermal stability of a silica-rich vanadium tailing
475 based geopolymer." *Construction and Building Materials*, Elsevier Ltd, 38, 43–47.

476 Kastiukas, G., Zhou, X., and Castro-Gomes, J. (2016). "Development and optimisation of
477 phase change material-impregnated lightweight aggregates for geopolymer composites
478 made from aluminosilicate rich mud and milled glass powder." *Constr. Build. Mater.*,

110, 201–210.

Khater, H. M. (2013). “Effect of silica fume on the characterization of the geopolymer materials.” *International Journal of Advanced Structural Engineering*, 5(1), 12.

Li, X., Wang, Z., and Jiao, Z. (2013). “Influence of curing on the strength development of calcium-containing geopolymer mortar.” *Materials*, 6(11), 5069–5076.

Mikulčić, H., Vujanović, M., Fidaros, D. K., Priesching, P., Minić, I., Tatschl, R., Duić, N., and Stefanović, G. (2012). “The application of {CFD} modelling to support the reduction of {CO2} emissions in cement industry.” *Energy*, 45(1), 464–473.

Mo, B., Zhu, H., Cui, X., He, Y., and Gong, S. (2014). “Effect of curing temperature on geopolymerization of metakaolin-based geopolymers.” *Appl. Clay Sci.*, 99, 144–148.

Murray, H. (2002). “Industrial clays case study.” *Min. Miner. Sust. Dev*, 1(64), 1–9.

Napp, T. A., Gambhir, A., Hills, T. P., Florin, N., and Fennell, P. S. (2014). “A review of the technologies, economics and policy instruments for decarbonising energy-intensive manufacturing industries.” *Renewable and Sustainable Energy Reviews*, 30, 616–640.

Neupane, K. (2016). “‘Fly ash and {GGBFS} based powder-activated geopolymer binders: A viable sustainable alternative of portland cement in concrete industry.’” *Mechanics of Materials*, 103, 110–122.

Pacheco-Torgal, F., Castro-Gomes, J., and Jalali, S. (2007). “Investigations about the effect of aggregates on strength and microstructure of geopolymeric mine waste mud binders.” *Cem. Concr. Res.*, 37(6), 933–941.

Pacheco-Torgal, F., Castro-Gomes, J., and Jalali, S. (2009a). “Tungsten mine waste geopolymeric binder: Preliminary hydration products investigations.” *Constr. Build. Mater.*, 23(1), 31–48.

Pacheco-Torgal, F., Castro-Gomes, J. P., and Jalali, S. (2008). “Investigations on mix design of tungsten mine waste geopolymeric binder.” *Constr. Build. Mater.*, 22(9), 1939–1949.

Pacheco-Torgal, F., Castro-Gomes, J. P., and Jalali, S. (2009b). “Utilization of_mining wastes to produce geopolymer binders.” *Geopolymers: Structures, Processing, Properties and Industrial Applications*, J. Provis and J. S. J. Van Jaarsveld, J.G.S., Van Deventer, eds., Woodhead Publishing Limited, 267–293.

Praprotnik, M., Janezic, D., and Mavri, J. (2004). “Temperature Dependence of Water Vibrational Spectrum: A Molecular Dynamics Simulation Study.” *J. Phys. Chem. A*, 108(50), 11056–11062.

Provis, J. L., Lukey, G. C., and Van Deventer, J. S. J. (2005). “Do geopolymers actually contain nanocrystalline zeolites? a reexamination of existing results.” *Chem. Mater.*, 17(12), 3075–3085.

Rahman, A., Rasul, M. G., Khan, M. M. K., and Sharma, S. (2016). “Chapter 9 - Cement Kiln Process Modeling to Achieve Energy Efficiency by Utilizing Agricultural Biomass as Alternative Fuels.” *Thermofluid Modeling for Energy Efficiency Applications*, M. M. K. Khan and N. M. S. Hassan, eds., Academic Press, 197–225.

Sarkar, M., Dana, K., and Das, S. (2015). “Microstructural and phase evolution in metakaolin geopolymers with different activators and added aluminosilicate fillers.” *Journal of Molecular Structure*, Elsevier B.V, 1098, e147–e153.

Shao, Y., Lefort, T., Moras, S., and Rodriguez, D. (2000a). “Studies on concrete containing

ground waste glass." *Cem. Concr. Res.*, 30(1), 91–100.

Shao, Y., Lefort, T., Moras, S., and Rodriguez, D. (2000b). "Studies on concrete containing ground waste glass." *Cement and Concrete Research*, article, 30(1), 91–100.

Silva, I., Castro-Gomes, J., and Albuquerque, A. (2012a). "Mineral Waste Geopolymeric Artificial Aggregates as Alternative Materials for Wastewater-Treatment Processes: Study of Structural Stability and pH Variation in Water." *Journal of Materials in Civil Engineering*, 24(6), 623–628.

Silva, I., Castro-Gomes, J. P., and Albuquerque, A. (2012b). "Effect of immersion in water partially alkali-activated materials obtained of tungsten mine waste mud." *Constr. Build. Mater.*, article, 35, 117–124.

Szczepańska, J., and Twardowska, I. (2004). "III.6 - Mining waste." *Solid Waste: Assessment, Monitoring and Remediation*, Waste Management Series, I. Twardowska, ed., Elsevier, 319–385.

Telesca, A., Marroccoli, M., Ibris, N., Lupiáñez, C., Díez, L. I., Romeo, L. M., and Montagnaro, F. (2017). "Use of oxyfuel combustion ash for the production of blended cements: A synergetic solution toward reduction of {CO2} emissions." *Fuel Processing Technology*, 156, 211–220.

Temuujin, J., Williams, R. P., and van Riessen, A. (2009). "Effect of mechanical activation of fly ash on the properties of geopolymer cured at ambient temperature." *Journal of Materials Processing Technology*, article, 209(12–13), 5276–5280.

Thomas, R. J., and Peethamparan, S. (2015). "Alkali-activated concrete: Engineering properties and stress–strain behavior." *Construction and Building Materials*, Elsevier Ltd, 93, 49–56.

Ye, J., Zhang, W., and Shi, D. (2014). "Effect of elevated temperature on the properties of geopolymer synthesized from calcined ore-dressing tailing of bauxite and ground-granulated blast furnace slag." *Construction and Building Materials*, 69, 41–48.

Yellishetty, M., Karpe, V., Reddy, E. H., Subhash, K. N., and Ranjith, P. G. (2008). "Reuse of iron ore mineral wastes in civil engineering constructions: A case study." *Resources, Conservation and Recycling*, 52(11), 1283–1289.

Zhang, L., Ahmari, S., and Zhang, J. (2011). "Synthesis and characterization of fly ash modified mine tailings-based geopolymers." *Constr. Build. Mater.*, 25(9), 3773–3781.

Zhang, S. A. K. P. L. (2014). "Alkali Activation of Copper Mine Tailings and Low-Calcium Flash-Furnace Copper Smelter Slag." *Journal of Materials in Civil Engi- neering*, 27(6), 1–11.

564 **Table 1.** Chemical Composition (wt.%) of raw TMW, WG determined by SEM-EDX

Chemical compound	**TMW (%)**	**TMW S.D**	**WG (%)**
Na_2O	1.31	1.45	9.72
MgO	1.01	2.98	0.00
Al_2O_3	21.06	2.53	0.00
SiO_2	47.88	3.86	73.93
SO_3	8.72	2.83	0.00
K_2O	4.12	0.78	0.69
Fe_2O_3	9.97	2.73	0.40
P_2O_5	0.00	0.27	0.00
CaO	0.88	0.99	12.83
TiO_2	0.66	0.35	0.00

565

566

567 **Table 2.** Summary of preparation and curing regimes for the variables studied

Sample	Activator mixing time (mins)	Curing temperature (°C)	Oven curing duration(hours)
M2.5	2.5	60	24
M5	5		
M10	10		
M15	15		
M20	20		
T20	5	20	24
T40		40	
T60		60	
T80		80	
D4	5	80	4
D12			12
D24			24
D36			36

568
569
570

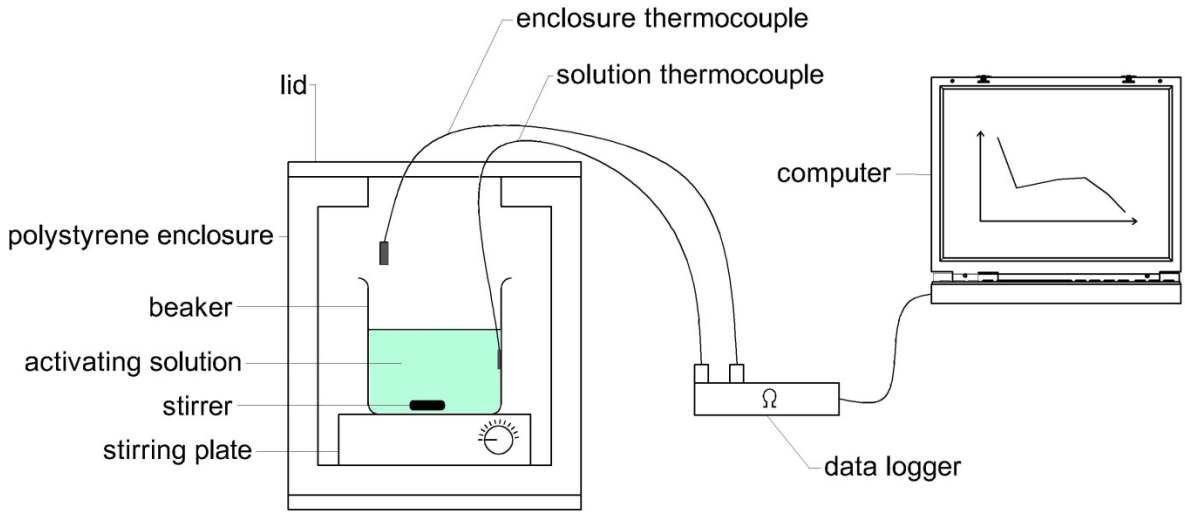

571

572 **Fig.1** SS/SH activator solution temperature measurement set up

573

574

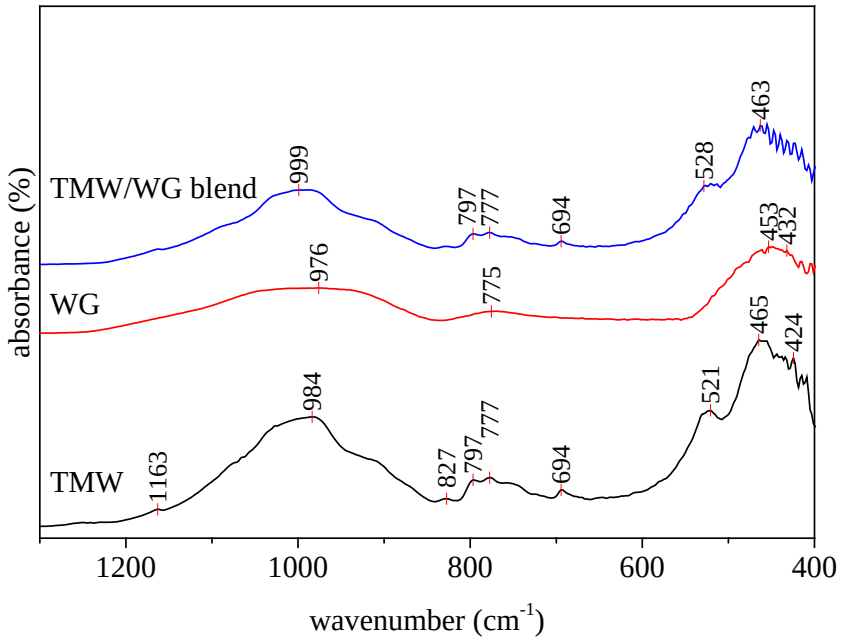

575

576 **Fig.2** ATR-FTIR absorbance spectra of the as received raw TMW, WG, and TMW-WG

577 blend (80 and 20% mass fractions, respectively)

578

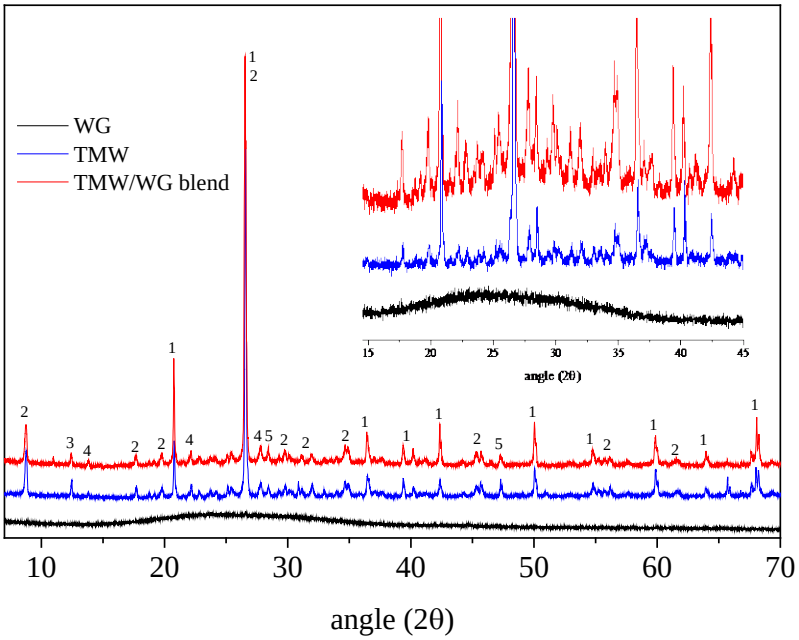

579

580 **Fig.3** XRD patterns of TMW, WG and blended TMW/WG WG (1- silica, 2- muscovite, 3-

581 sodium aluminosilicate, 4- rudashevskyite, 5- pyrite)

582

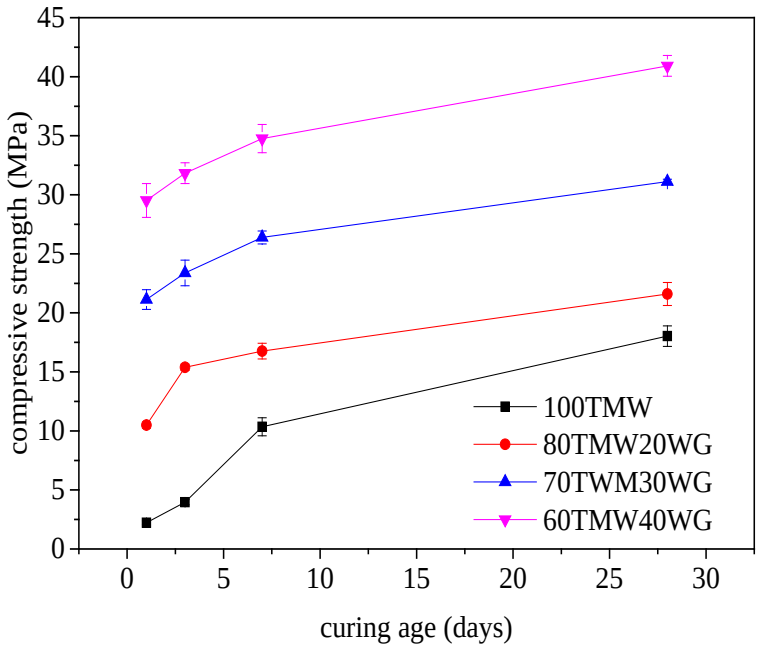

583

584 **Fig.4** Effects of WG substitution on TMW AAB compressive strength

585

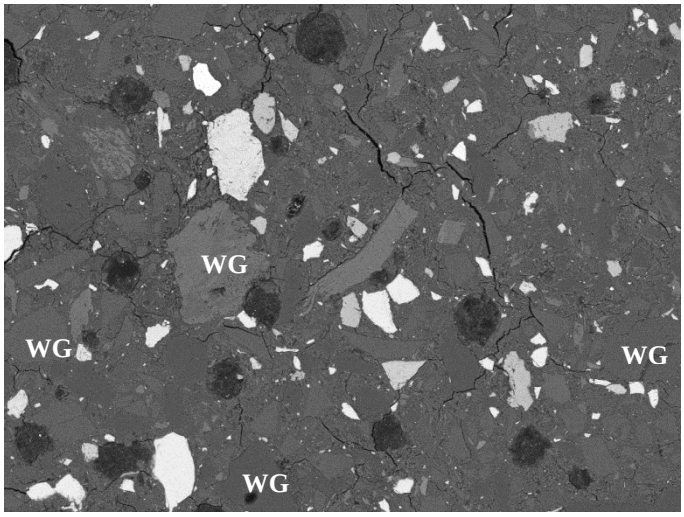

586

587 **Fig.5** Polished thin-section of TMW-WG AAB with 40 wt.% WG at 28-days

588

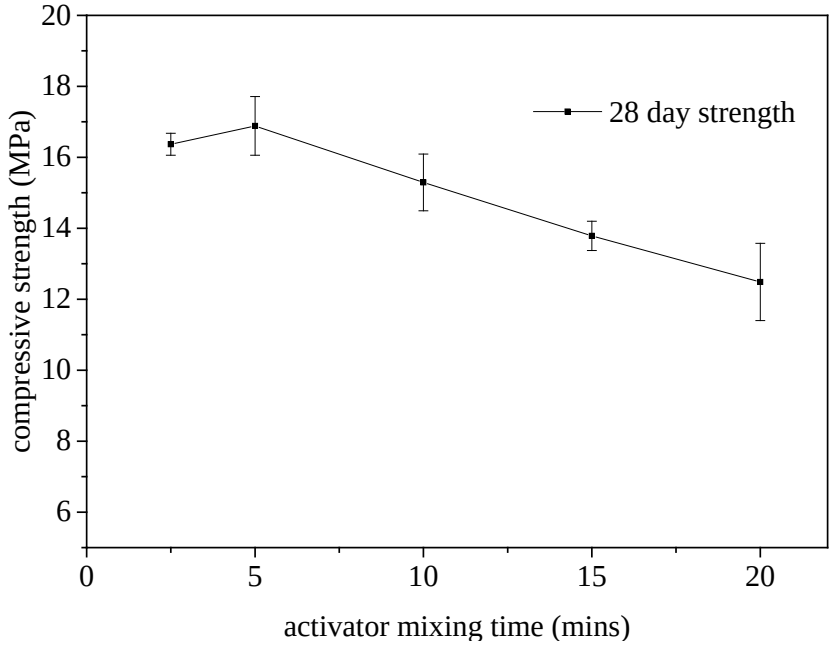

589

590 **Fig.6** Effect of SS/SH activator solution mixing time on 28-day compressive strength of

591 TMW-WG ABB cured at 60ºC for 24 hours

592

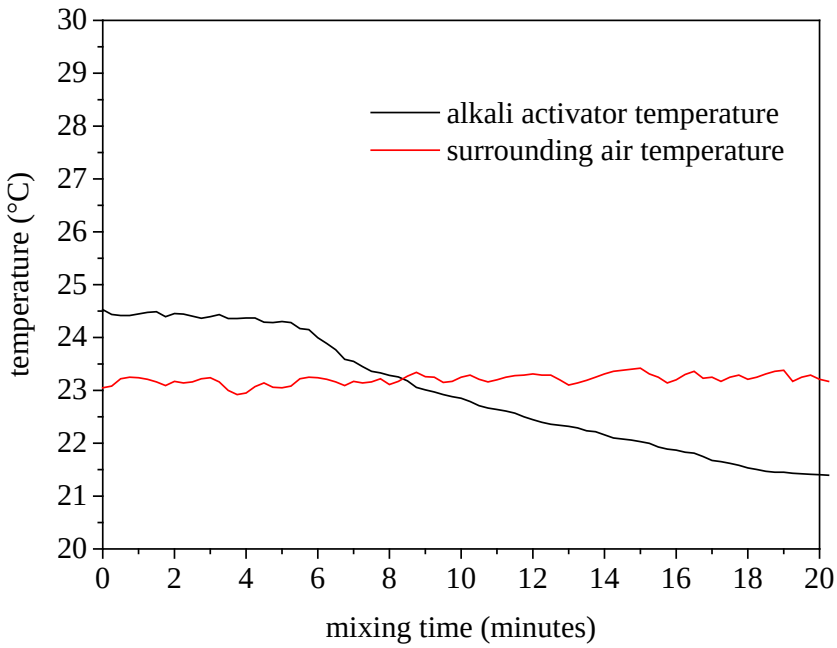

593

594 **Fig.7** SS/SH activator solution temperature due to prolonged mixing

595

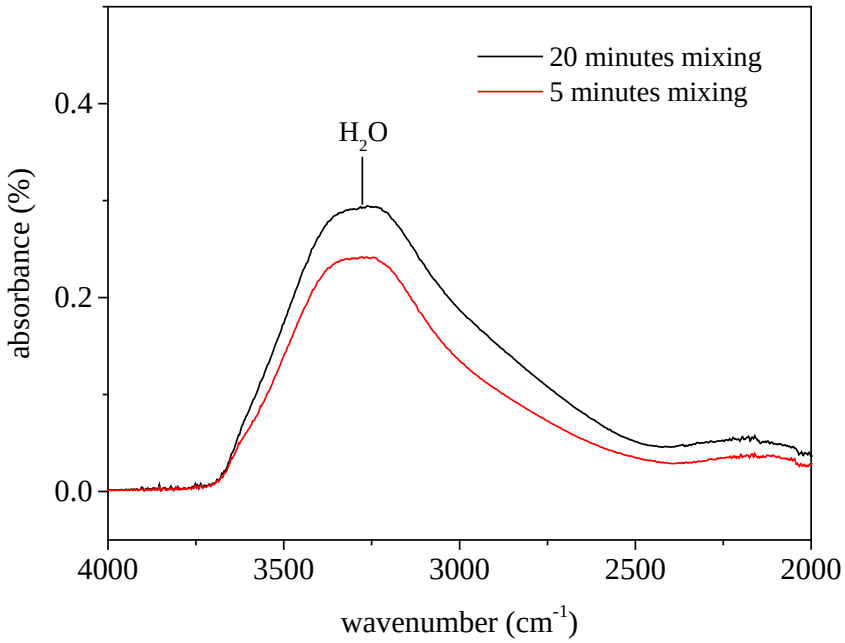

596

597 **Fig.8** ATR-FTIR spectrum of SS/SH activator solution with varying mixing time

598

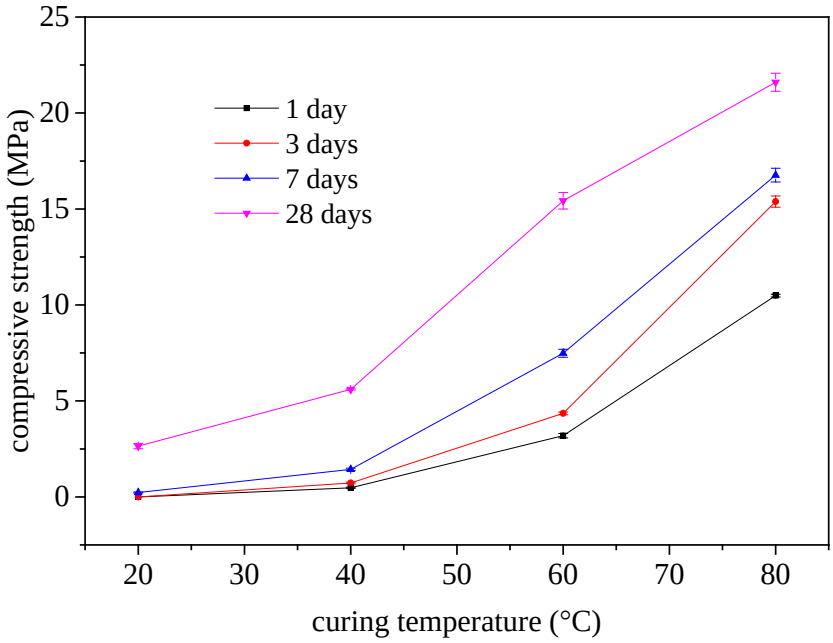

Fig.9 TMW-WG AAB compressive strength (1-28d), for samples cured for 24 h at 20, 40, 60 and 80ºC.

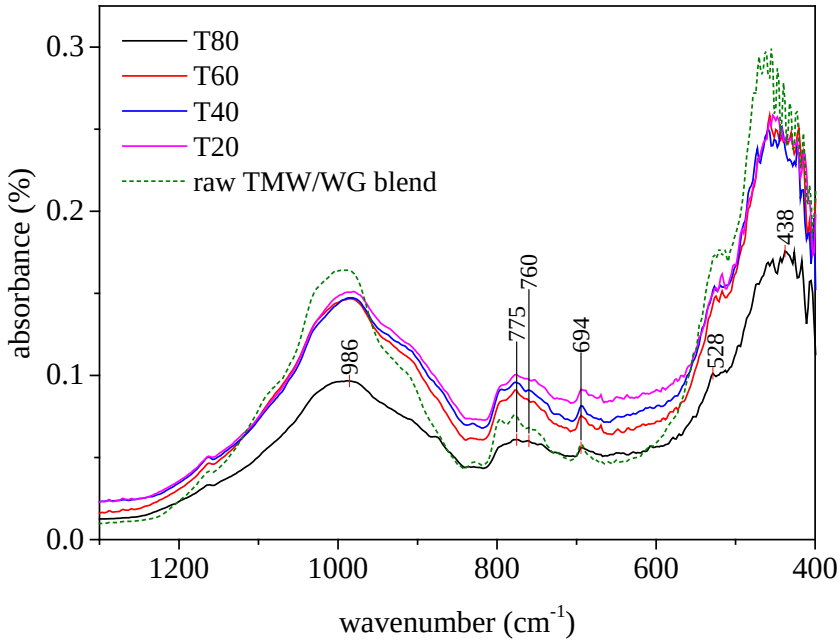

603

604 **Fig.10** ATR-FTIR absorbance spectra of as received raw TMW/WG and TMW-WG AAB at

605 28 days cured at 40, 60 and 80°C

606

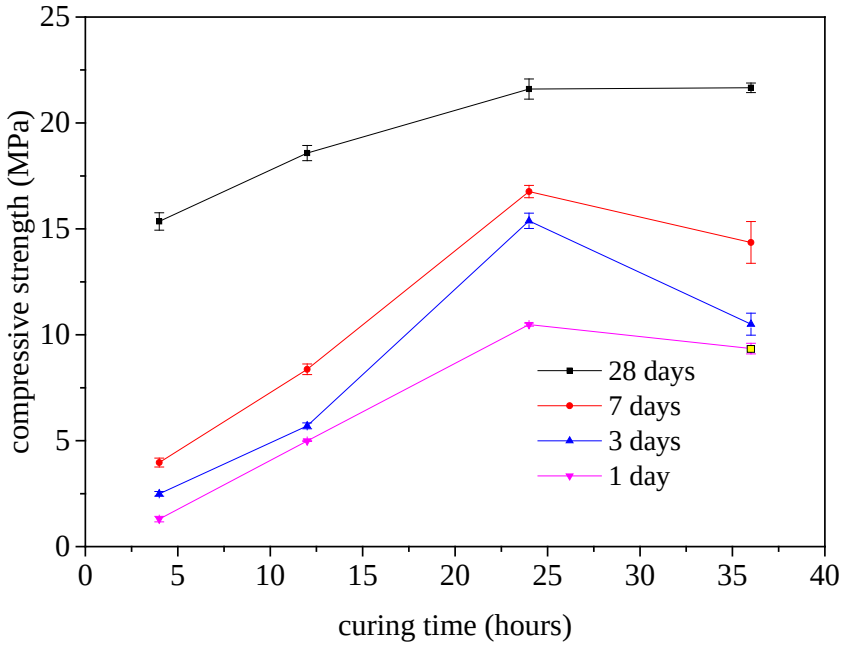

607

608 **Fig.11** TMW-WG AAB compressive strength (1-28d), for samples cured at 80ºC for 4, 12,

609 24 and 36 h.

610

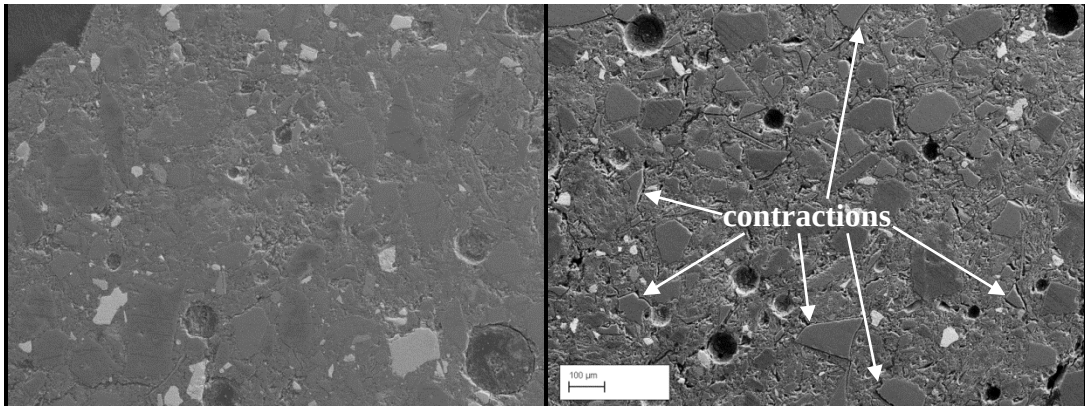

Fig.12 TMW-WG ABB sample cured at 80°C for (a) 24 h and (b) 36 h

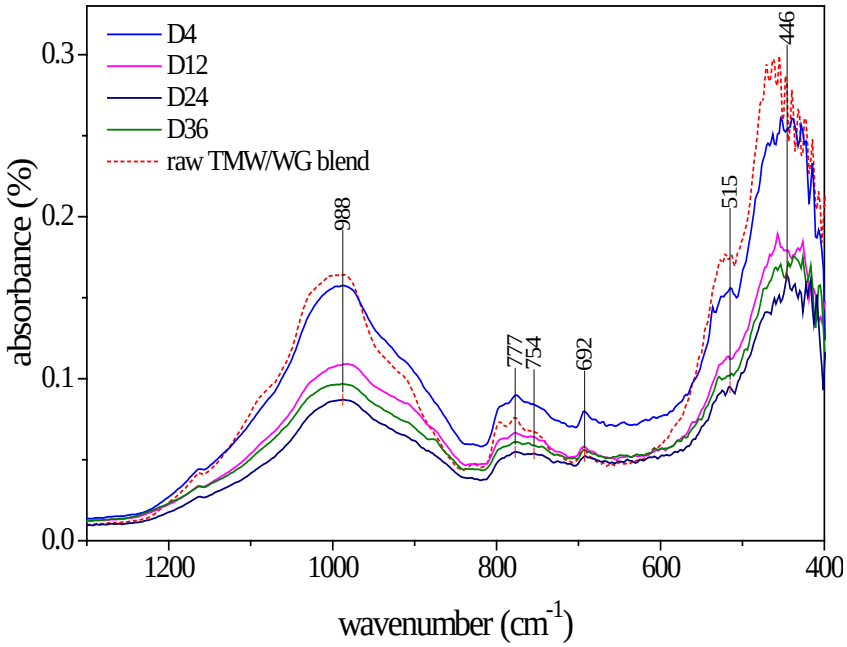

614

615 **Fig.13** ATR-FTIR absorbance spectra of as received raw TMW/WG and TMW-WG AAB at

616 28 days cured at 80°C for 4, 12, 24 and 36 h.

617